applied optics

Numerical simulations of holographic spatiospectral traces of spatiotemporally distorted ultrashort laser pulses

ZHE GUANG,* MICHELLE RHODES, AND RICK TREBINO

School of Physics, Georgia Institute of Technology, 837 State Street, Atlanta, Georgia 30332, USA
**Corresponding author: zguang3@gatech.edu*

Received 27 April 2015; revised 26 June 2015; accepted 26 June 2015; posted 29 June 2015 (Doc. ID 239762); published 21 July 2015

We simulate traces for a catalog of spatiotemporally complex pulses measured using a single-shot complete spatiotemporal pulse-measurement technique we recently developed, called Spatially and Temporally Resolved Intensity and Phase Evaluation Device: Full Information from a Single Hologram (STRIPED FISH). The only such technique ever developed to our knowledge, STRIPED FISH measures the complete spatiotemporal intensity $I(x,y,t)$ and phase $\phi(x,y,t)$ of an arbitrary laser pulse using an experimentally recorded trace consisting of multiple digital holograms, one for each frequency present in the pulse. To understand the effects of various spatiotemporal distortions on the STRIPED FISH trace, we numerically investigate STRIPED FISH trace features for a catalog of pulses, including the spatially and temporally transform-limited pulse, temporal and spatial double pulses, spherically focusing and diverging pulses, self-phase modulated and self-focusing pulses, spatiotemporally coupled pulses, and pulses with complex structures. As a practical example, we also analyze an experimentally recorded trace of a focusing pulse with spatial chirp. Overall, we find that, from STRIPED FISH's informative trace, significant spatiotemporal characteristics of the unknown pulse can be immediately recognized from the camera frame. This, coupled with its simple pulse-retrieval algorithm, makes STRIPED FISH an excellent technique for measuring and monitoring ultrafast laser sources.

OCIS codes: (320.0320) Ultrafast optics; (320.7100) Ultrafast measurements.

http://dx.doi.org/10.1364/AO.54.006640

1. INTRODUCTION

Many of the greatest scientific discoveries have resulted directly from more powerful methods for measuring light. Among these discoveries are the detection of finely resolved spectral lines from atomic transitions that led to the theory of quantum mechanics and the discovery of DNA using x-ray crystallography, not to mention the essential contributions of telescopes and microscopes to science as we know it. Therefore, developing ever more informative and powerful techniques for measuring light is an important endeavor. Indeed, most naturally occurring light is broadband and hence has ultrafast variations in time which, as a result, cannot currently be measured without resorting to statistical measures. Thus, ultrafast light measurement is one of the key frontiers in light-measurement science. As always, it is best to begin with the simplest of such waveforms, the ultrashort laser pulses [1,2], which are generally quite simple but can potentially contain some complexities in both space and time. Due to their ultrafast nature, these pulses are difficult to measure—so much so that, for the first several decades of research in this field, researchers made do with only rough estimates of the pulse duration available from nonlinear optical autocorrelation methods [3–5]. It was not until the early 1990s that a technique emerged to measure the actual pulse temporal intensity and phase, $I(t)$ and $\phi(t)$ [6–8]. This method, Frequency-Resolved Optical Gating (FROG), has been adapted to characterize pulses from nanosecond to attosecond durations [9,10] and from infrared to deep ultraviolet wavelengths [11–13], but it and other methods that have followed [14–16] must assume a smooth profile over space [17]. Unfortunately, however, pulse temporal quantities often depend on transverse position, a phenomenon called spatiotemporal couplings (STCs), and only a few techniques [18,19] can measure even simple first-order STCs [20].

Measuring STCs is all the more important because deliberately introducing them into the pulse for practical reasons is common. For example, in pulse-shaping applications, angularly dispersive components such as gratings or prisms are typically used [21–23] to couple the light's temporal or frequency profile with its spatial or angular profile [24], so that modified or even exotic pulse shapes can be generated, greatly increasing the

diversity of ultrashort-pulse applications. Another example is the accurate manipulation of STCs to allow focusing of pulses to very small, intense foci [25–27] with reduced longitudinal focal regions, which has important applications in microscopy and microfabrication.

Meanwhile, from another perspective, many interesting ultrafast phenomena inherently exhibit complex spatiotemporal structures. Filamentation, in which nonlinear optical effects interact with diffractive effects, allows a beam to propagate with roughly unchanged beam size over a significant distance [28]. Little is known, still, of such a beam's precise space and time shapes. Also, Bessel pulses are of great interest to scientists because of their light bullet behavior and superluminal propagation speed [29]. However, such pulses also exhibit complex spatiotemporal structures that need to be thoroughly characterized.

On the other hand, STCs can be harmful in some cases if not properly eliminated. For example, in chirped pulse amplification, the presence of residual STCs due to misalignment is highly undesirable because they can greatly lengthen the pulse and decrease the peak power [28,30]. This is also true in spatiotemporal focusing. Although accurate STC manipulations can focus pulses to small foci, alignment is critical and even STCs introduced by lenses can easily distort the short pulses [31,32]. As a result, in general laser applications, it is essential to measure the complete spatiotemporal field in order to guarantee a promised pulse profile or to prevent undesired pulse distortions.

Furthermore, it is far preferable to know the pulse's spatiotemporal profile on a *single-shot* and in real time. This is because instability is often present in ultrashort pulses, and if a measurement requires an average over many pulses, it cannot yield correctly the pulse because it averages over different pulses and the measurement can only return one. Unfortunately, most measurement methods—even those that measure only the temporal variations of the pulse—are multishot. Worse, it has recently been shown that most recently developed temporal measurement methods, when confronted with an unstable train of pulses, measure only the well-known and infamous coherent artifact and so yield an erroneously short and simple pulse [33–35]. Fortunately, for some temporal-intensity and phase-measurement techniques such as FROG, independent checks exist and the stability of the pulse train can be ascertained. Furthermore, single-shot measurement is possible [33,34]. However, for spatiotemporal measurement methods, this has not been the case. So far, essentially all complete spatiotemporal methods are multishot and require performing spatial or spectral scans [36–38]. Therefore, single-shot spatiotemporal pulse characterization is necessary, especially for potentially unstable pulses such as extremely intense pulses from low-rep-rate amplification systems. Also, monitoring the pulse's spatiotemporal profile in real time can help experimentalists distinguish possible problems, quickly make adjustments, and reach decisions. Again, this is possible only if the pulse's complete spatiotemporal information is fully recorded on a single shot.

To meet all these needs, our group has recently introduced a pulse measurement technique called Spatially and Temporally Resolved Intensity and Phase Evaluation Device: Full Information from a Single Hologram (STRIPED FISH) [39,40]. STRIPED FISH uses a single camera frame to record multiple digital holograms, each at a different frequency, revealing the spatiospectral profile of an unknown pulse. As a result, it can operate single-shot. It also uses a FROG-measured, spatially filtered reference pulse which, in the case of pulse averaging, performs the task of determining stability of the pulse train before the pulse even enters the STRIPED FISH device. Understanding STRIPED FISH traces can help us identify the spatiotemporal structure of unknown pulse in the experiment simply by visually inspecting the live camera frame, even though the full retrieval algorithm is also direct and fast.

Indeed, it is very important that all pulse-measurement techniques have a catalog of simulated traces for a range of typical pulses [35,41] in order to better understand the technique's features and issues and to prevent possible misinterpretations, which have occurred many times in the field of ultrashort-laser-pulse measurement in the past due to its many subtleties. Consequently, in this paper we provide such a catalog. We begin our discussion by reviewing the general concept and retrieval algorithm of STRIPED FISH. Then we look at the assumptions used in the simulations and discuss the effects of spatiospectral pulse profiles on the holographic trace. After that, we simulate traces for a catalog of typical pulses, including a transform-limited pulse, temporal and spatial double pulses, spherically focusing or diverging pulses, self-phase modulated and self-focusing pulses, first-order spatiotemporally coupled pulses, and pulses with complicated structures. Finally, as a practical example, we investigate an experimentally recorded trace and compare it with the corresponding simulated trace. With these analyses, we show that STRIPED FISH is a good candidate for measuring and monitoring the spatiotemporal characteristics of ultrashort pulses.

2. STRIPED FISH

Spectrally resolved digital holography has been applied to retrieve the spatiotemporal field of light [42,43]. Specifically, to obtain the full spatiotemporal information, holograms of different frequencies need to be recorded between the unknown pulse and a known reference pulse. Then, for each hologram (off-axis holography by angle θ), the unknown spatiospectral field $E_{unk}(x, y, \omega_i)$ at one frequency ω_i is encoded in the integrated intensity $I(x, y, \omega_i)$:

$$\begin{aligned} I(x,y,\omega_i) = {} & |E_{unk}(x,y,\omega_i)|^2 + |E_{\mathrm{ref}}(x,y,\omega_i)|^2 \\ & + E_{unk}(x,y,\omega_i)E^*_{\mathrm{ref}}(x,y,\omega_i)\exp\left(+i\frac{y\omega_i}{c}\sin(\theta)\right) \\ & + E^*_{unk}(x,y,\omega_i)E_{\mathrm{ref}}(x,y,\omega_i)\exp\left(-i\frac{y\omega_i}{c}\sin(\theta)\right), \end{aligned} \tag{1}$$

where the interferometric term $E_{unk}(x, y, \omega_i)E^*_{\mathrm{ref}}(x, y, \omega_i)\exp(+i\frac{y\omega_i}{c}\sin(\theta))$ can be extracted by simple Fourier filtering [44]. Then the unknown field $E_{unk}(x, y, \omega_i)$ can be obtained with knowledge of the reference field [40]. By applying the same procedures for multiple digital holograms, the spatiospectral information of the unknown pulse can be obtained at

multiple frequencies. Afterward, the spatiotemporal field profile can be retrieved by inverse Fourier transform:

$$E_{unk}(x,y,t) = \frac{1}{2\pi}\int_{-\infty}^{+\infty} E_{unk}(x,y,\omega)\exp(i\omega t)\mathrm{d}\omega \approx \frac{1}{2\pi}\sum_i E_{unk}(x,y,\omega_i)\exp(i\omega_i t)\delta\omega. \quad (2)$$

To determine the reference pulse $E_{\mathrm{ref}}(x,y,\omega)$, part of the beam is sent through a spatial filter and then characterized by a FROG device, such as GRENOUILLE [14,45]. Using part of the same beam helps to guarantee that the spectrum of the reference pulse contains the spectrum of the unknown pulse, so all frequencies in the unknown pulse can be measured. The spatial filter eliminates the high-spatial-frequency components, yielding a spatially smooth beam whose temporal dependence is easy to accurately measure using FROG. As a result, the reference pulse field is completely known in both space and time (frequency). Specifically, the reference pulse field at frequency ω_i then has the form $E_{\mathrm{ref}}(x,y,\omega_i) = E_{\mathrm{ref}}(x,y)|_{\omega_i} E_{\mathrm{ref}}(\omega_i)$ and is STC-free.

To obtain multiple holograms at different frequencies, wavelength scanning can be performed on the unknown and reference pulses, as was done in Ref. [42], but this is inherently multishot. More recently, using diffractive optics, angular wavelength-resolving components, and inexpensive high-pixel-count cameras, we showed that it is possible to illuminate different regions of the camera frame with digital holograms at different frequencies [39,40,46,47]. As shown in Fig. 1(a), the incoming beam pairs are first diffracted into multiple orders and then spectrally filtered into different frequencies by a bandpass filter. The unknown and reference beams cross at a small vertical angle on the camera frame, yielding simultaneously the desired holograms at different locations. By rotating the coarse grating slightly (and maintaining it at this fixed rotation angle), the array of holograms on any given laser shot is tilted slightly [see Fig. 1(b)], so that each beam pair enters the bandpass filter at a different angle, which, because the filter's transmission wavelength is mainly horizontal angle dependent [31], yields holograms at different colors and no two holograms have the same color. Note that in our simulation, we use false colors to clearly indicate the different frequencies among holograms. However, in real experiment, a camera only sensitive to pixel saturation will only "see" the recorded integrated intensity, as shown in Fig. 1(c). To guarantee the intensity homogeneity among the diffraction orders, we also incorporate imaging optics and an apodizing filter [40]. With the knowledge of the previously measured reference pulse, this simple device can measure the unknown pulse's complete spatiotemporal profile, following the algorithm described before. The resulting camera frame of multiple different-color holograms is called the STRIPED FISH trace.

3. ASSUMPTIONS AND DISCUSSION

To intuitively show the effects of STCs on the STRIPED FISH trace, we have made a few assumptions for our numerical simulations. First, we assume that, if only the STC-free reference pulse is recorded by STRIPED FISH (that is, the unknown pulse is blocked), all of the diffraction orders in the STRIPED FISH trace would have the same intensity, as in Fig. 2(a). This effectively means that the trace is normalized to the spectrum of the reference pulse. Under this assumption, if an unknown pulse with the same spectrum is measured, all the holograms will still show the same peak intensity. Experimentally, the imaging optics and apodizing filter attempt to make this a reality [40]. Even if the intensities of all diffracted orders are not ideally equal, one can always numerically normalize the recorded values afterward. By making this assumption, however, the intensity variation effects

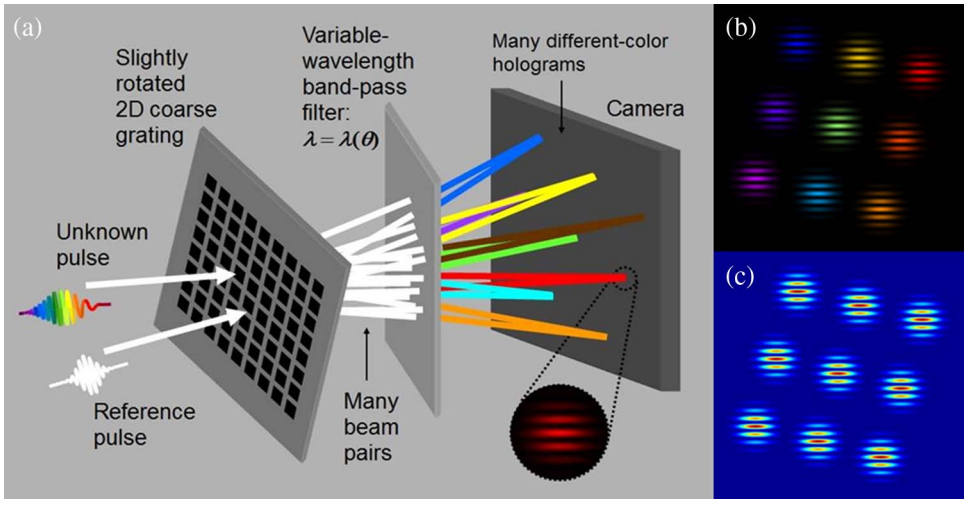

Fig. 1. STRIPED FISH apparatus and traces. (a) Conceptual plot of STRIPED FISH. An unknown pulse and a reference pulse are combined into the apparatus, diffracted, spectrally filtered, and finally imaged onto the camera frame, forming holograms at different frequencies. Imaging optics are omitted for simplicity. (b) STRIPED FISH trace is tilted due to the slight rotation of the coarse grating. Each hologram has a different incident angle to the filter, yielding a different frequency. Hereafter, we use false colors in our simulation to interpret different frequencies of holograms. (c) However, in a real experiment with a monochromatic camera, these different frequencies will only be encoded by different orders of holograms, and the color scale of the camera frame is often used for the recorded integrated intensity value.

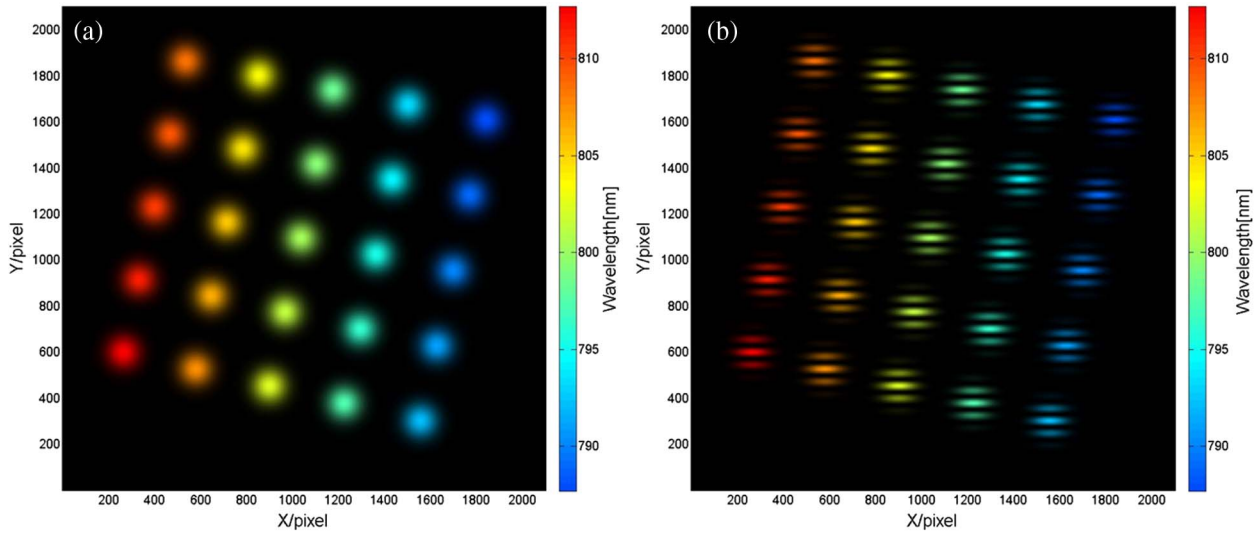

Fig. 2. (a) Spatiospectral intensity trace (without reference pulse) and (b) STRIPED FISH trace (with reference pulse) for a Gaussian-shaped transform-limited pulse in space and time. Note that the holograms have equal intensities at all wavelengths, indicated by their brightness and colors. The x and y axes are in 10 μm pixel increments.

brought up by the spatiotemporal complexities in the unknown pulse on the STRIPED FISH trace can be clearly shown. In each STRIPED FISH trace we assume 25 holograms, forming a 5 × 5 matrix, each with a different monochromatic wavelength evenly ranging over 25 nm, with the central wavelength λ_0 being 800 nm.

As a STRIPED FISH trace is generated by spatially interfering an unknown beam with a reference beam at each frequency, the trace itself reveals the spatiospectral characteristics of the unknown pulse. As summarized in Table 1, the unknown pulse spatial structure is contained within each hologram: the spatial intensity is represented by the intensity distribution and the spatial phase is indicated by the fringe shape within one hologram. Likewise, the spectral information is reflected by multiple holograms: the spectral intensity is represented by the intensity variations and the spectral phase is indicated by the fringe shifts among different holograms. When STC exists in the unknown pulse, the STRIPED FISH trace shows correlations between the spatial and spectral effects, which we will discuss later.

4. PULSE TRACE SIMULATIONS

A. Transform-limited Pulse

First, we investigate the simple case when the unknown pulse is a transform-limited Gaussian pulse in both space and time. The expression for such a spatiotemporal field is

$$E(x, y, t) = E(x, y)E(t) = \exp(-ax^2 - by^2) \times \exp(-ct^2) \quad (3)$$

where the parameters a, b, and c are related to the pulse's intensity FWHM spatial widths Δx, Δy, and temporal width Δt by $\Delta x = \sqrt{\frac{2\ln(2)}{a}}$, $\Delta y = \sqrt{\frac{2\ln(2)}{b}}$, and $\Delta t = \sqrt{\frac{2\ln(2)}{c}}$. And note that we hereafter omit the optical carrier-frequency term for all electric fields. We will also omit the subscript indicating the unknown field, as all fields henceforth will refer to the unknown field (to be measured).

The Fourier transform versus t of Eq. (3) gives us the spatiospectral field

$$E(x, y, \omega) = E(x, y)E(\omega) = \sqrt{\frac{\pi}{c}} \exp(-ax^2 - by^2) \times \exp\left(-\frac{\omega^2}{4c}\right) \quad (4)$$

In this case, a, b, and c are all defined to be real quantities ($1\ \text{mm}^{-2}$, $1\ \text{mm}^{-2}$, and $2.04 \times 10^{-4}\ \text{fs}^{-2} = 1/(70\ \text{fs})^2$; $\Delta x = 1.18$ mm, $\Delta y = 1.18$ mm, and $\Delta t = 82.4$ fs), so the pulse is collimated and transform-limited, with no temporal chirp or STC. To emphasize the effects of the unknown pulse, we use the above assumptions to plot the simulated traces. A spatiospectral intensity trace of the transform-limited pulse is plotted in Fig. 2(a), which is the camera trace when no reference pulse is incident. Figure 2(b) shows the equal-intensity STRIPED FISH holograms. In the pictures, color denotes the wavelength and brightness the intensity.

Table 1. Spatial and Spectral Effects of the Unknown Pulse on the STRIPED FISH Trace

Spatial	Amplitude	Intensity distribution within one hologram
	Phase	Fringe shape within one hologram
Spectral	Amplitude	Intensity among multiple holograms
	Phase	Fringe shift among multiple holograms

B. Temporal and Spatial Double Pulses

To better illustrate the effects in Table 1, we now simulate the cases of temporal double pulses and synchronized, spatially separated pulses. The STRIPED FISH traces are shown in Fig. 3.

The temporal double pulses, each of which is transform-limited, share the same intensity. One pulse is delayed by τ (136 fs) from the other, with a π phase jump in between. To show the spectral-phase variation, we set their arrival time

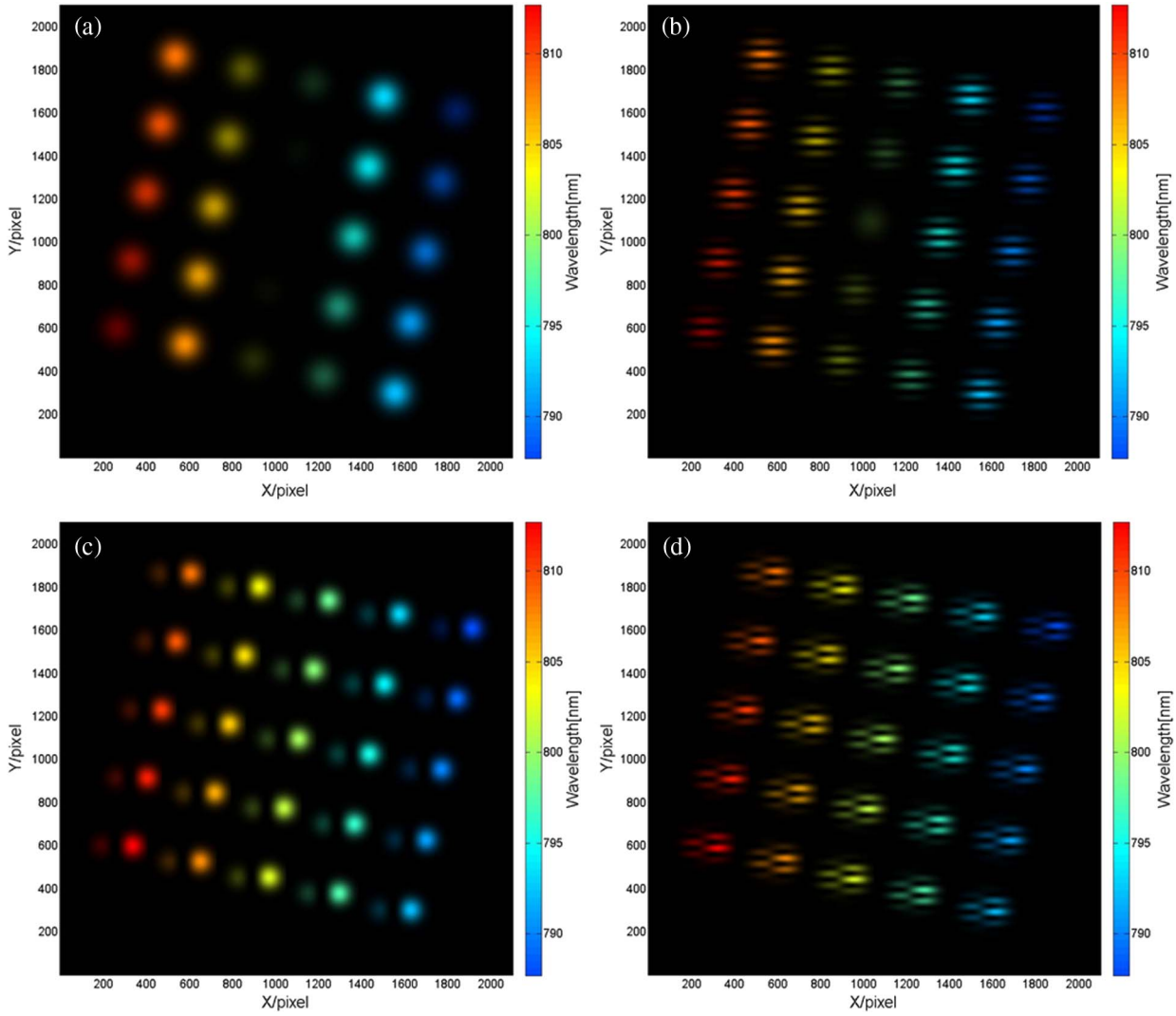

Fig. 3. Spatiospectral intensity traces (without reference pulses) and STRIPED FISH traces (with reference pulses) for double pulses. (a) Spatiospectral intensity trace of a temporal double pulse, with equal-intensity individual pulses and a π phase jump between them. (b) STRIPED FISH trace of the temporal double pulse in (a). (c) Spatiospectral intensity trace of a spatial double pulse, with the left pulse one fourth the intensity of the right pulse. A π phase jump occurs between the two pulses. (d) STRIPED FISH trace of the spatial double pulses shown in (c).

to be t_0 (209 fs), so that they have a linearly varying spectral phase. The expression for the unknown pulse field is

$$E(x,y,t) = \exp(-ax^2 - by^2)\exp[-c(t+t_0)^2] + \exp(i\pi)\exp(-ax^2 - by^2)\exp[-c(t+t_0+\tau)^2]. \quad (5)$$

From Fig. 3(a), we can see the variation in the spectral intensity of the double pulse. And from Fig. 3(b), we can clearly see the corresponding spectral intensity variations among the different-color holograms. Also, the fringe positions vary from hologram to hologram in Fig. 3(b) [compared with Fig. 2(b)], indicating that the spectral phase of the unknown pulse changes with frequency.

Similarly, we demonstrate the spatial effects in STRIPED FISH traces by simulating a pair of synchronized and spatially separated pulses. Two beams are assumed to propagate in the same direction, the left of which has half the amplitude (and therefore a quarter of the intensity) of the right one. To show the spatial phase variation, we incorporate a π phase jump between the two component pulses. The expression is

$$E(x,y,t) = \exp[-a'(x-x_0)^2 - b'y^2]\exp(-ct^2) + 0.5\times\exp(i\pi)\exp[-a'(x+x_0)^2 - b'y^2]\exp(-ct^2), \quad (6)$$

where $a' = b' = 2.04\ \text{mm}^{-2}$ and $x_0 = 0.7$ mm. Figures 3(c) and 3(d) show that the left pulse is dimmer than the right one. Also, in the middle of each hologram in Fig. 3(d), we can clearly observe a fringe discontinuity due to the spatial phase jump.

C. Spherically Focusing or Diverging Pulses

Another interesting case is the focusing or diverging pulse. Focusing or diverging pulses, respectively, correspond to a

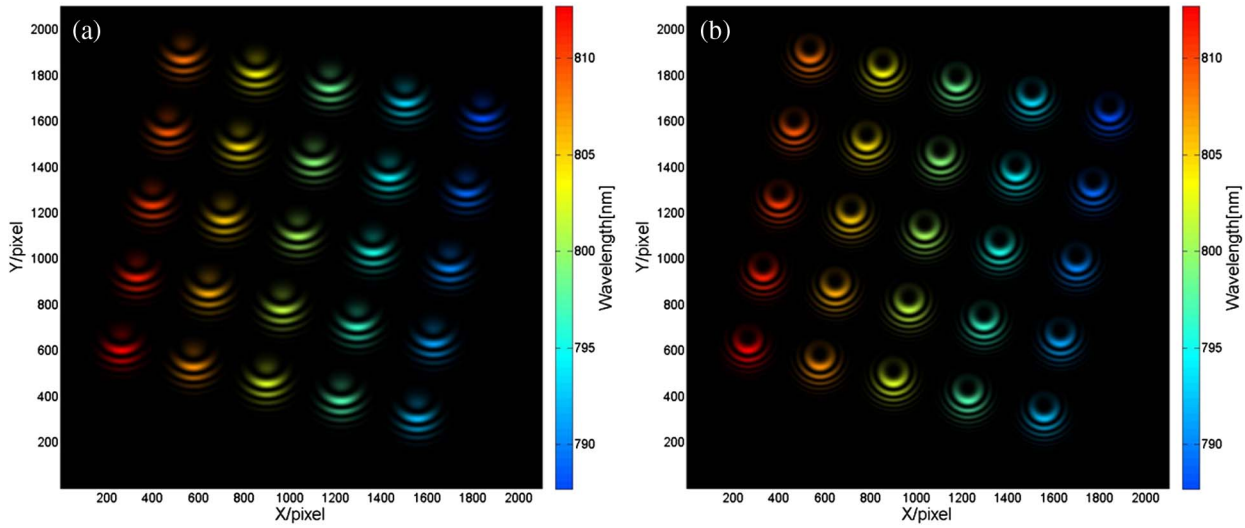

Fig. 4. STRIPED FISH traces for focusing pulses. (a) STRIPED FISH holograms for a loosely focusing pulse, with $R = -816$ mm. (b) STRIPED FISH holograms for a tightly focusing pulse, with $R = -408$ mm.

spatial quadratic phase function with radius $R < 0$ or $R > 0$. Note that in our simulations, the unknown pulse propagates on axis and the reference pulse crosses it from above. The field expression for a pulse with radius of curvature R is

$$E(x, y, \omega) = \exp\left(-ax^2 - by^2 - \frac{\omega^2}{4c} - \frac{i\omega}{2cR}(x^2 + y^2)\right). \quad (7)$$

As shown in Fig. 4, the curvature of the interference fringes indicates the wavefront curvature of the unknown pulse. The rings are not concentric because the unknown and reference beams also cross at a small vertical angle θ. The smaller value the focusing radius R is, the more tightly the pulse is focused and the more curved the fringes will be [see Fig. 4(b)]. In the opposite R case, when the pulse is diverging, the hologram fringes will be a vertically flipped version of Figs. 4(a) and 4(b) (thus not shown).

D. Self-Phase-Modulated and Self-Focused Pulse

Next, to investigate pulses with modifications in both the spatial and spectral profiles, we look at a pulse with one typical nonlinear optical effect, the intensity-dependent phase. When an intense pulse passes through an optical Kerr medium [48], self-phase modulation (SPM) can be observed in the time domain. The spatial counterpart, the self-focusing (SF), can also happen for ultrashort pulses with sufficient energy in their propagation through bulk solids, liquids, and gases [49]. Such a pulse with SPM and SF has an approximate expression:

$$E(x, y, t) = \exp(-ax^2 - by^2 - ct^2)\exp(-in_2 I), \quad (8)$$

where the intensity term $I = |\exp(-ax^2 - by^2 - ct^2)|^2$. Note that, for simulation purposes, we have used normalized field amplitude and (therefore) intensity, with dimensionless, unity peak values. Also, we use a numerical index n_2 to characterize the amount of introduced phase modulation. The resulting spatiospectral and STRIPED FISH traces are shown in Fig. 5, for 1.5 rad peak phase modulation. Note that the spectral intensity in the picture is dimmer in the middle orders than the side ones. This shows a spectral-broadening effect caused by SPM: due to intensity-dependent temporal phase, the pulse energy has been redistributed toward the edges of the spectrum, so central spectrum appears dimmer after normalization. The slight fringe curvature inside each hologram in Fig. 5(b) indicates the spatial self-focusing, and the effect is more evident again in side orders than the middle ones as a result of the intensity-dependent phase modulation.

E. Spatiotemporally Coupled Pulses

Now we discuss the effects of first-order STCs on STRIPED FISH traces. To begin with, because the STRIPED FISH trace comprises holograms in the spatiospectral domain, we first look at spatial chirp (SPC) and wavefront tilt dispersion (WFD), which correspond to the real and imaginary STC terms in the spatiospectral field [50]. The effect of SPC along the x and y directions are similar, and therefore we only show the SPC along x in Fig. 6. The corresponding expression is

$$E(x, y, \omega) = \exp(-ax^2 - by^2)\exp(2x\omega\mathrm{SPC}) \times \exp\left(-\frac{\omega^2}{4 \times (-i\mathrm{TCP} + c)}\right), \quad (9)$$

where a, b, and c are defined as before, and SPC and TCP are the spatial chirp and temporal chirp (14 fs/mm and 1×10^{-4} fs^{-2}, respectively). As expected, the spatial chirp causes holograms of different frequencies to shift linearly in space with their corresponding frequencies.

Shown in Figs. 7(a) and 7(b) are traces for WFD (−35 fs/mm) along the x and y directions, respectively. Only STRIPED FISH traces (holograms) are plotted, because WFD is a phase term not visible in the unknown pulse spatiospectral intensity. Thus, the center positions of the holograms are not shifted. The WFD along the x direction causes the fringes to rotate, changing their orientations; however, the WFD along the y direction causes the spacing between fringes to vary, decreasing monotonically from red to blue. Note also that, for collimated beams, WFD is related to angular

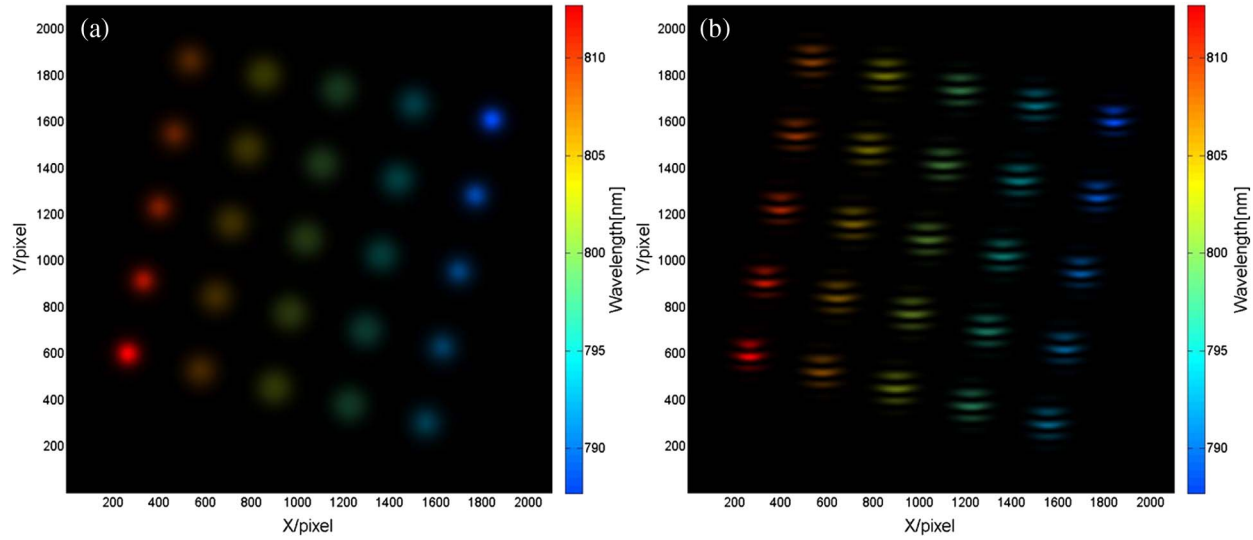

Fig. 5. Spatiospectral intensity trace (without reference pulse) and STRIPED FISH trace (with reference pulse) for the pulse with SPM and SF ($n_2 = 1.5$). (a) Spatiospectral intensity of the unknown pulse. The intensity is normalized so the brightness shows the relevant intensities. Note that the bluest and reddest orders have the highest intensity due to SPM. (b) STRIPED FISH holograms. Note that the SF effect is indicated by the curvature of fringes in each hologram.

dispersion (AGD) [50]. The expressions for the WFD pulses are

$$E(x, y, \omega) = \exp(-ax^2 - by^2)\exp(2ix\omega\,\mathrm{WFD}) \times \exp\left(-\frac{\omega^2}{4 \times (-i\mathrm{TCP} + c)}\right), \quad (10)$$

$$E(x, y, \omega) = \exp(-ax^2 - by^2)\exp(2iy\omega\,\mathrm{WFD}) \times \exp\left(-\frac{\omega^2}{4 \times (-i\mathrm{TCP} + c)}\right). \quad (11)$$

Now we note that, to first order, all STCs in all four domains (temporal, spectral, spatial, and spatial frequency) are interrelated by Fourier transforms [50]. Given the beam parameters and STC terms in one particular domain, the STC values in all other FT-related domains can be uniquely determined. In our case, as the STRIPED FISH trace exists in the spatiospectral ($x\omega$) domain, the parameters that sufficiently define the pulse are beam spot size, wavefront curvature, bandwidth and frequency chirp, and the coupling terms SPC and WFD. Therefore, from another perspective, the presence of STCs in other FT-related domains [spatiotemporal (xt), spatial-frequency-temporal (kt), and spatial-frequency-spectral

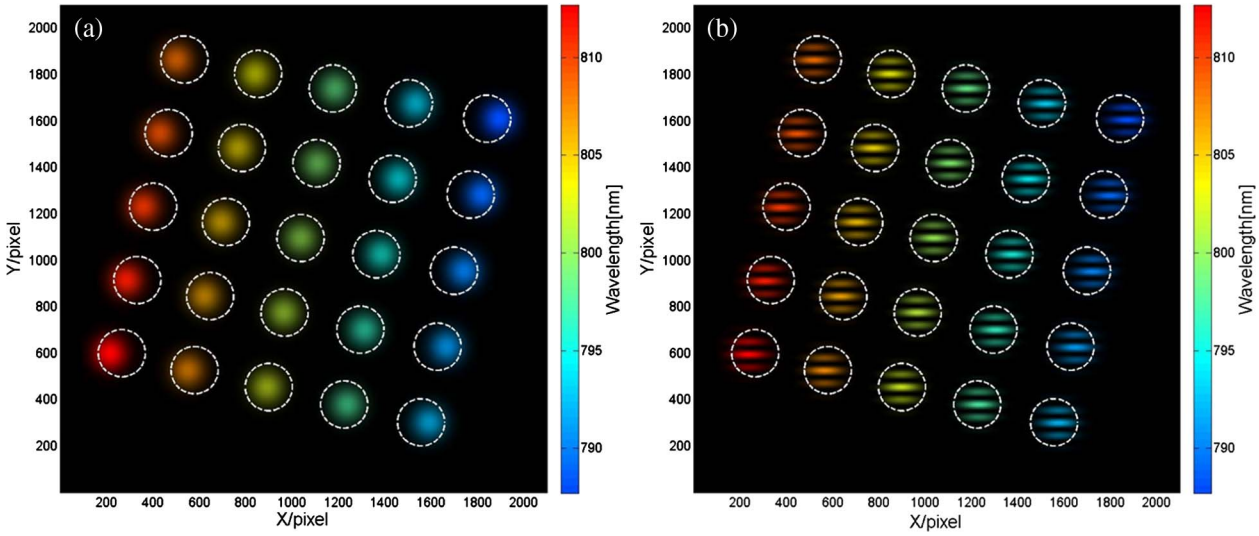

Fig. 6. Spatiospectral intensity trace (without reference pulse) and STRIPED FISH trace (with reference pulse) for the spatially chirped pulse. The white circular contours indicate the central positions of the holograms in the transform-limited case (no SPC) or effectively the central positions of the reference pulse. (a) Spatiospectral intensity of the pulse with SPC along the x direction. (b) STRIPED FISH holograms.

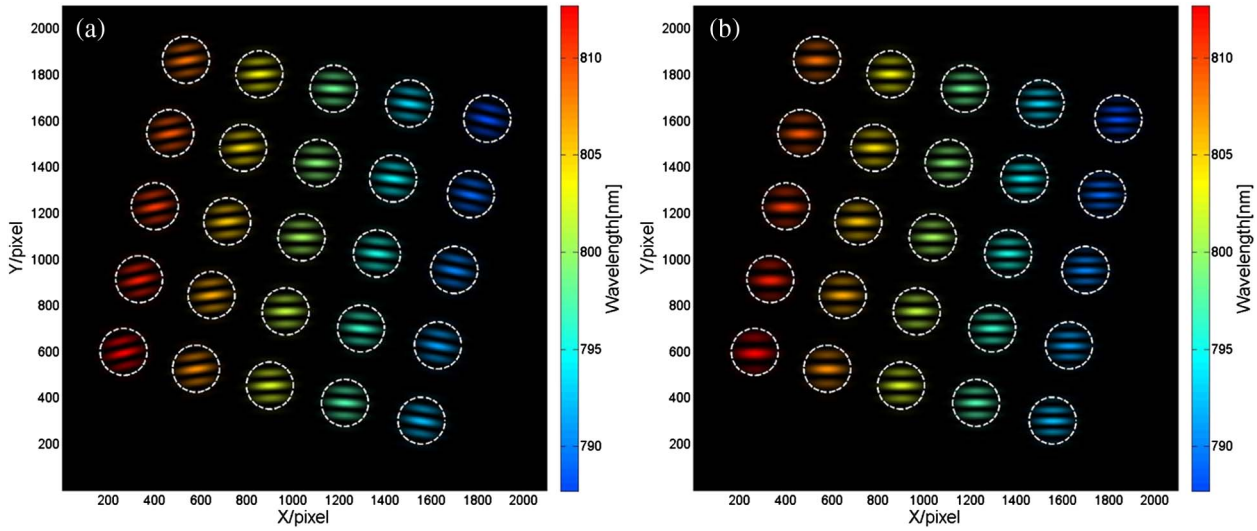

Fig. 7. STRIPED FISH traces for the wavefront-tilt-dispersed pulse. White circular contours indicate the central positions of the transform-limited case (no WFD). (a) STRIPED FISH holograms of a pulse with WFD along x. (b) STRIPED FISH holograms of a pulse with WFD along y.

domains ($k\omega$)] will be visible in the spatiospectral domain and thus be recorded by the STRIPED FISH trace. As an example we investigate a common STC, pulse-front tilt (PFT). The traces of PFT (50 fs/mm, normalized by the pulse width) along x or y are shown in Figs. 8(a) and 8(b), respectively. Specifically, their expressions are

$$E(x,y,t) = \exp(-ax^2 - by^2)\exp(2xt\,\mathrm{PFT}) \times \exp(-ct^2 + i\mathrm{TCP}t^2), \quad (12)$$

$$E(x,y,t) = \exp(-ax^2 - by^2)\exp(2yt\,\mathrm{PFT}) \times \exp(-ct^2 + i\mathrm{TCP}t^2). \quad (13)$$

Applied along the x direction, the effect of PFT shows the combination of the two "fundamental" effects of SPC and WFD shown above. That is, central positions of holograms shift and their fringe orientations vary with frequency. Likewise, when applied along y, PFT shifts the central y positions of the holograms and also varies the fringe spacing. This is in accordance with the discussions in Ref. [51]: PFT can result from AGD or simultaneous SPC and TCP.

F. Simultaneous Cases: Focusing Pulses with STCs

Lenses or focusing mirrors are often used to focus pulses with STCs. For instance, in the typical pulse-shaping geometry, focusing lenses are used to convert angular dispersion to spatial chirp; after passing through the spatial light modulator, the beam propagates through a reverse geometry to undo the effects of the earlier optics [52,53]. Therefore, we now investigate the STRIPED FISH traces for focusing STCs. We use the same values as before for STCs, and $R = -1632$ mm for pulse

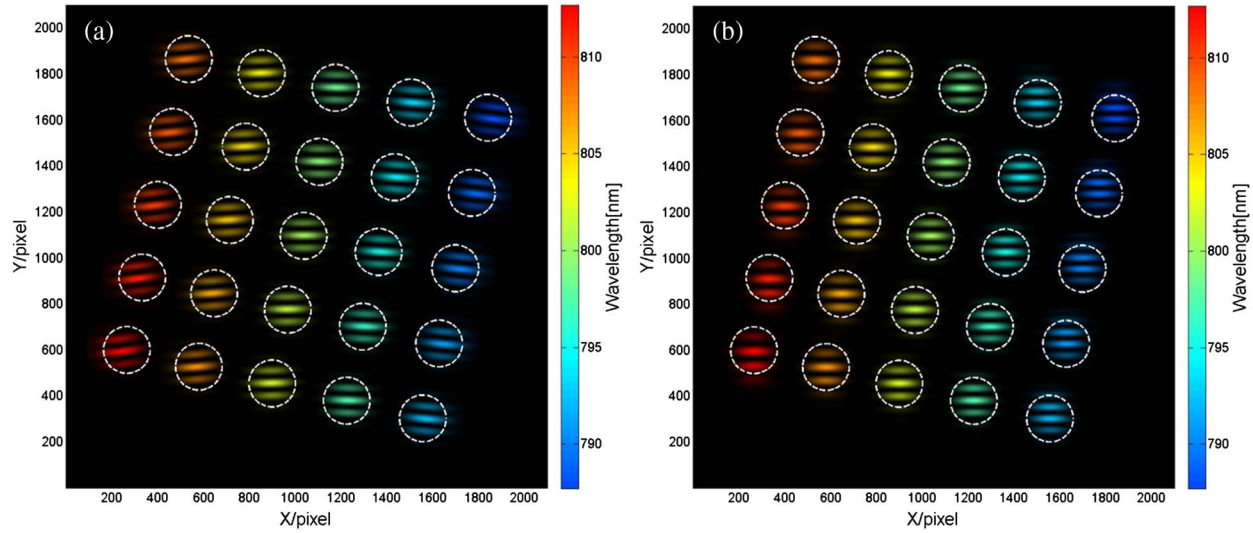

Fig. 8. STRIPED FISH traces for pulsefront tilted pulses. (a) STRIPED FISH holograms of a pulse with PFT along x. (b) STRIPED FISH holograms of a pulse with PFT along y.

focusing. Figures 9(a) and 9(b) show the STRIPED FISH traces for focusing SPC, along the x and y directions, respectively. Due to the SPC, central positions of the holograms shift with frequencies. Also, the fringes are curved, indicating that the unknown pulse is focusing. Note that in Fig. 9(a), the fringe orientations have seemingly rotated, due to visual artifacts caused by the horizontally shifted intensities. In Figs. 9(c) and 9(d), STRIPED FISH traces for focusing pulses with WFD along x or y are shown. Central positions of these holograms are not shifted. The fringes, either changing their orientations or spacing with respect to frequency, all present curved patterns, which indicates the curved wavefront.

G. Pulses with Complex Structures

To show an example of complex intensity and phase variations, we incorporate a pulse with hypothetical third-order distortions in the spatiospectral domain. The resulted STRIPED FISH trace in Fig. 10 shows the complexity of the pulse, clearly different from any pulse investigated previously. The mathematical expression of the unknown pulse is

$$E(x, y, \omega) = \exp(-ay^2 - bx^2 + iC_0\omega(x^2 + y^2)) \exp\left(-\frac{\omega^2}{4c}\right), \tag{14}$$

where a, b, c, and C_0 are defined to be 1 mm^{-2}, 4 mm^{-2}, 2.04×10^{-4} fs^{-2}, and 0.1, respectively. Although complicated, the hologram structures can still be analyzed following the rules stated before. In Fig. 10, both the spatiospectral intensity trace and the STRIPED FISH hologram trace show beam patterns with a wider span in the y than in the x direction, indicating different beam widths. Although the spatiospectral intensity trace shows the same pattern for all wavelengths (which indicates an identical spectral intensity profile as the Fourier-transform-limited reference pulse), the STRIPED FISH holograms show fringes that vary from order to order.

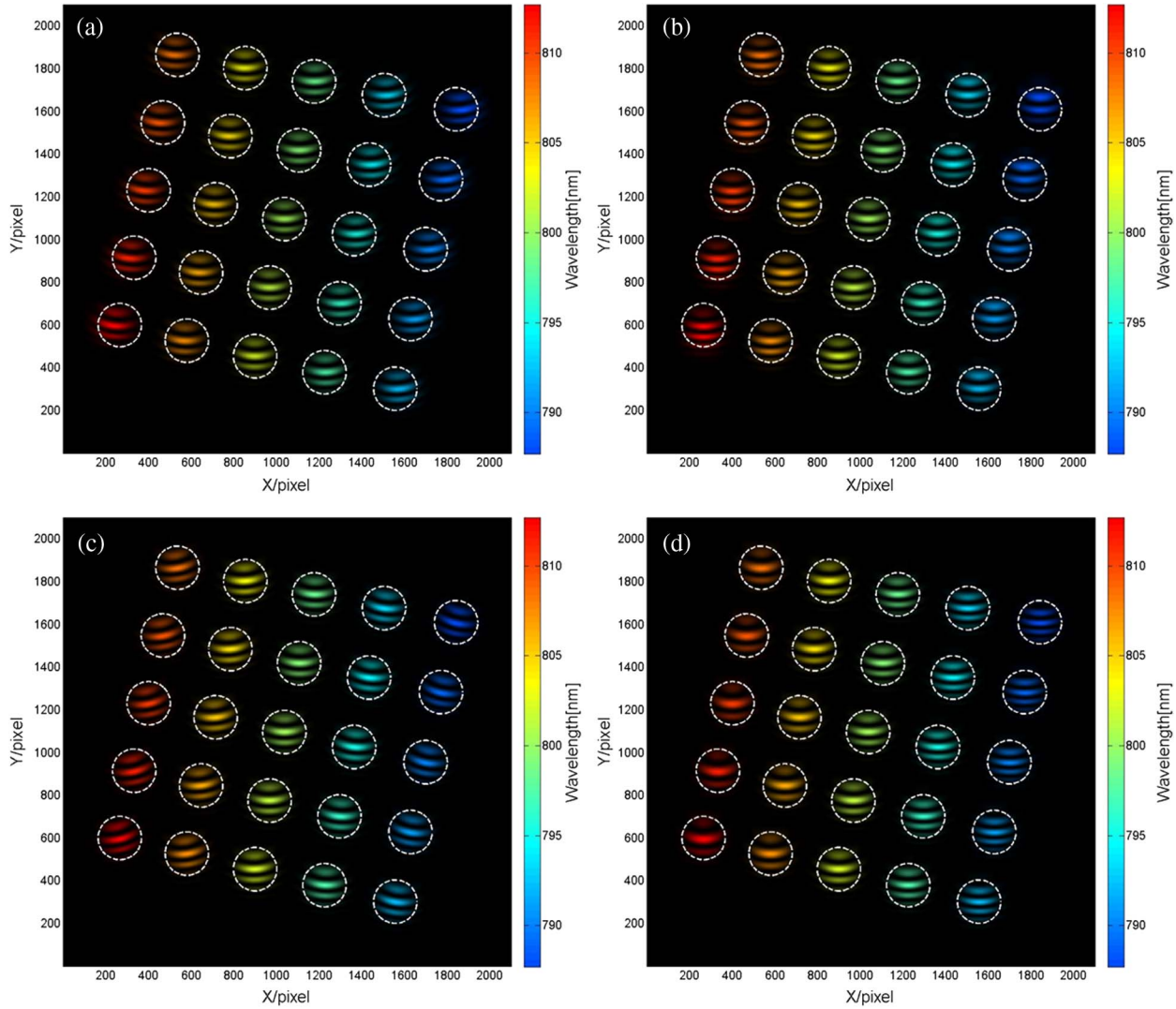

Fig. 9. STRIPED FISH traces for a focusing pulse with STCs. (a) STRIPED FISH holograms of a focusing pulse with SPC along x. The rotation of fringe orientations is due to the shifting of the central position of the unknown pulse. (b) STRIPED FISH holograms of a focusing pulse with SPC along y. (c) STRIPED FISH holograms of a focusing pulse with WFD along x. (d) STRIPED FISH holograms of a focusing pulse with WFD along y.

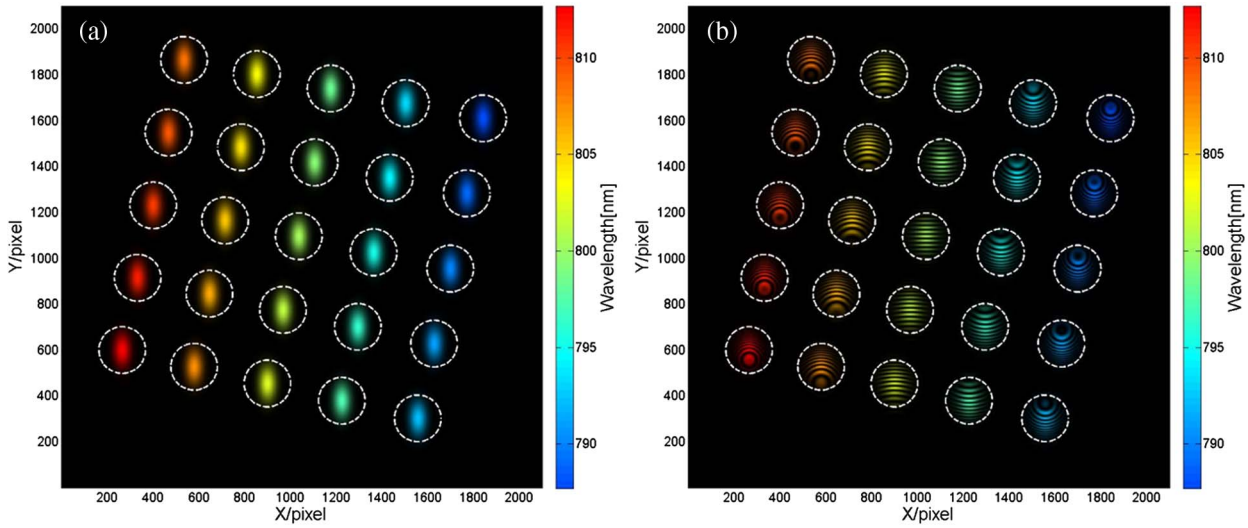

Fig. 10. Spatiospectral intensity trace (without reference pulse) and STRIPED FISH trace (with reference pulse) of a pulse with hypothetical third-order distortions. Note that the fringes are distorted in an unprecedented manner. (a) Spatiospectral intensity of the unknown pulse. (b) STRIPED FISH holograms.

The middle-frequency hologram (green) shows essentially no curvature, and therefore is close to collimation. The low-frequency hologram (red) shows downward curvature which corresponds to a diverging wavefront, and the high-frequency hologram (blue) shows a focusing wavefront. So mainly the quadratic spatial phase depends on frequency, which is a third-order (at least) phase effect. The center positions of the holograms are not shifted and their fringe orientations are not tilted, indicating no SPC or WFD along x. However, it is hard to tell if the unknown pulse contains WFD along y from the trace.

In this manner, a measured STRIPED FISH trace can be interpreted for the unknown pulse's spatiospectral information. Of course, as the STRIPED FISH trace contains the complete information about the unknown pulse, we can run the full retrieval algorithm to yield values for arbitrarily high-order terms (versus x, y, and t or ω) by polynomial-fitting the resulting field.

H. Experimental Example

We now demonstrate an example of experimentally recorded STRIPED FISH trace. The trace is associated with a focusing pulse with SPC along x. Such a pulse profile is introduced by a prism pair and followed by a focusing lens. In the STRIPED FISH trace (Fig. 11), we can see the STC effects. The intensity of the holograms is fairly even across the trace, suggesting no evident modifications to the reference spectrum. Curved and nearly circular fringes mean that the pulse presents a focusing quadratic spatial phase. Central positions of holograms have small hologram-dependent shifting, and therefore the fringes

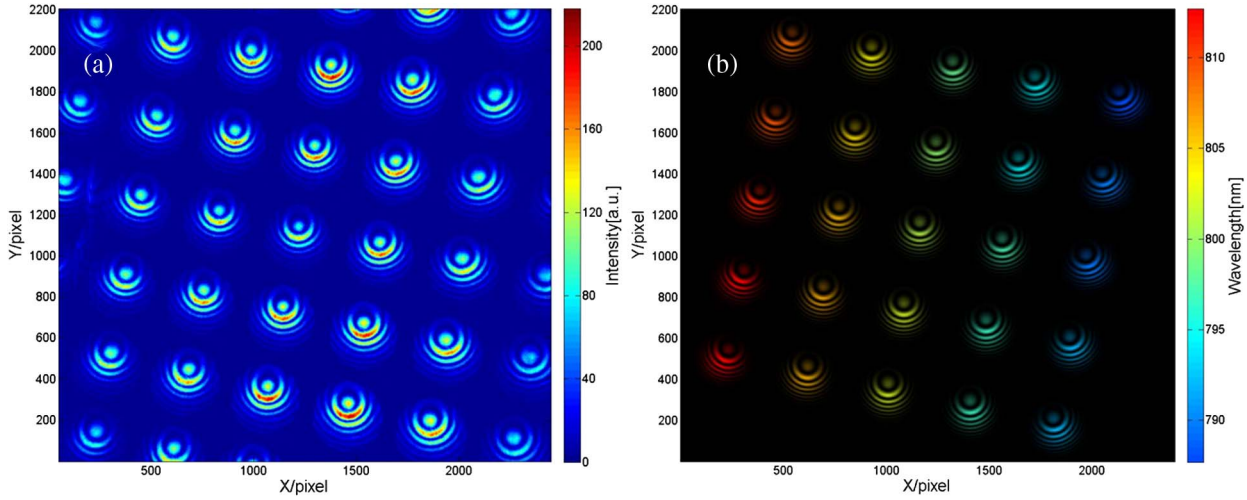

Fig. 11. STRIPED FISH trace experiment example. (a) Recorded STRIPED FISH holograms for a focusing pulse with SPC along x. Color scale indicates intensity on the camera. (b) Simulated STRIPED FISH holograms. Color scale indicates wavelengths recorded from experiment.

show slight rotations from the left side to the right side. This agrees with our introduction of spatial chirp into the beam. Thus, the experimental trace matches our expectations from the experimental setup. Moreover, we have performed numerical simulations for the trace, based on the parameters obtained from the experiment, which also show good agreement.

5. CONCLUSION

With its simple and compact apparatus, STRIPED FISH is a convenient single-shot technique for measuring the complete spatiotemporal field of pulses. Its spatiospectral experimental trace, a set of holograms generated at various frequencies by spatially crossing the reference beam with the unknown beam, is highly informative and needs to be understood. Though a robust pulse-retrieval algorithm can easily extract the complete field information from the STRIPED FISH trace, one can gain much insight immediately about the unknown pulse profile simply by visually inspecting the STRIPED FISH trace on the camera. The STRIPED FISH trace contains (for each frequency) the spatial information of the unknown pulse in one particular hologram, and it records (for each location) the spectral profiles of the unknown pulse among multiple holograms. To help determine the spatiotemporal profile of the unknown pulse, we have simulated STRIPED FISH traces for typical pulse species, where considerably different holographic traces are analyzed in detail. We also show hypothetical and experimental pulse traces to demonstrate what to look for if the pulse contains spatiotemporal complexity. Because the STRIPED FISH trace can be inspected in real time, STRIPED FISH can thus be very useful for measuring or monitoring spatiotemporal profiles of ultrashort pulses.

Funding. Georgia Research Alliance (GRA); National Science Foundation (NSF) (ECCS-1307817).

REFERENCES

1. F. McClung and R. Hellwarth, "Giant optical pulsations from ruby," J. Appl. Phys. **33**, 828–829 (1962).
2. J. A. Wheeler, A. Borot, S. Monchocé, H. Vincenti, A. Ricci, A. Malvache, R. Lopez-Martens, and F. Quéré, "Attosecond lighthouses from plasma mirrors," Nat. Photonics **6**, 829–833 (2012).
3. J. Giordmaine, P. Rentzepis, S. Shapiro, and K. Wecht, "Two-photon excitation of fluorescence by picosecond light pulses," Appl. Phys. Lett. **11**, 216–218 (1967).
4. J. Armstrong, "Measurement of picosecond laser pulse widths," Appl. Phys. Lett. **10**, 16–18 (1967).
5. K. Sala, G. Kenney-Wallace, and G. Hall, "CW autocorrelation measurements of picosecond laser pulses," IEEE J. Quantum Electron. **16**, 990–996 (1980).
6. R. Trebino, *Frequency-Resolved Optical Gating: The Measurement of Ultrashort Laser Pulses* (Kluwer, 2002).
7. D. J. Kane and R. Trebino, "Characterization of arbitrary femtosecond pulses using frequency resolved optical gating," IEEE J. Quantum Electron. **29**, 571–579 (1993).
8. R. Trebino, K. W. DeLong, D. N. Fittinghoff, J. N. Sweetser, M. A. Krumbügel, and D. J. Kane, "Measuring ultrashort laser pulses in the time-frequency domain using frequency-resolved optical gating," Rev. Sci. Instrum. **68**, 3277–3295 (1997).
9. Y. Mairesse and F. Quéré, "Frequency-resolved optical gating for complete reconstruction of attosecond bursts," Phys. Rev. A **71**, 011401 (2005).
10. P. Bowlan and R. Trebino, "Complete single-shot measurement of arbitrary nanosecond laser pulses in time," Opt. Express **19**, 1367–1377 (2011).
11. F. Quéré, Y. Mairesse, and J. Itatani, "Temporal characterization of attosecond XUV fields," J. Mod. Opt. **52**, 339–360 (2005).
12. K. Michelmann, T. Feurer, R. Fernsler, and R. Sauerbrey, "Frequency resolved optical gating in the UV using the electronic Kerr effect," Appl. Phys. B **63**, 485–489 (1996).
13. B. A. Richman, M. A. Krumbügel, and R. Trebino, "Temporal characterization of mid-IR free-electron-laser pulses by frequency-resolved optical gating," Opt. Lett. **22**, 721–723 (1997).
14. P. O'Shea, M. Kimmel, X. Gu, and R. Trebino, "Highly simplified device for ultrashort-pulse measurement," Opt. Lett. **26**, 932–934 (2001).
15. J. Cohen, D. Lee, V. Chauhan, P. Vaughan, and R. Trebino, "Highly simplified device for measuring the intensity and phase of picosecond pulses," Opt. Express **18**, 17484–17497 (2010).
16. I. A. Walmsley and C. Dorrer, "Characterization of ultrashort electromagnetic pulses," Adv. Opt. Photon. **1**, 308–437 (2009).
17. D. Lee, Z. Wang, X. Gu, and R. Trebino, "Effect—and removal—of an ultrashort pulse's spatial profile on the single-shot measurement of its temporal profile," J. Opt. Soc. Am. B **25**, A93–A100 (2008).
18. S. Akturk, M. Kimmel, P. O'Shea, and R. Trebino, "Measuring spatial chirp in ultrashort pulses using single-shot frequency-resolved optical gating," Opt. Express **11**, 68–78 (2003).
19. S. Akturk, M. Kimmel, P. O'Shea, and R. Trebino, "Measuring pulse-front tilt in ultrashort pulses using GRENOUILLE," Opt. Express **11**, 491–501 (2003).
20. S. Akturk, X. Gu, P. Bowlan, and R. Trebino, "Spatio-temporal couplings in ultrashort laser pulses," J. Opt. **12**, 093001 (2010).
21. A. M. Weiner, J. P. Heritage, and E. Kirschner, "High-resolution femtosecond pulse shaping," J. Opt. Soc. Am. B **5**, 1563–1572 (1988).
22. R. L. Fork, C. H. Brito Cruz, P. Becker, and C. V. Shank, "Compression of optical pulses to six femtoseconds by using cubic phase compensation," Opt. Lett. **12**, 483–485 (1987).
23. S. Akturk, X. Gu, M. Kimmel, and R. Trebino, "Extremely simple single-prism ultrashort-pulse compressor," Opt. Express **14**, 10101–10108 (2006).
24. A. Kostenbauder, "Ray-pulse matrices: a rational treatment for dispersive optical systems," IEEE J. Quantum Electron. **26**, 1148–1157 (1990).
25. G. Zhu, J. Van Howe, M. Durst, W. Zipfel, and C. Xu, "Simultaneous spatial and temporal focusing of femtosecond pulses," Opt. Express **13**, 2153–2159 (2005).
26. F. He, H. Xu, Y. Cheng, J. Ni, H. Xiong, Z. Xu, K. Sugioka, and K. Midorikawa, "Fabrication of microfluidic channels with a circular cross section using spatiotemporally focused femtosecond laser pulses," Opt. Lett. **35**, 1106–1108 (2010).
27. D. N. Vitek, E. Block, Y. Bellouard, D. E. Adams, S. Backus, D. Kleinfeld, C. G. Durfee, and J. A. Squier, "Spatio-temporally focused femtosecond laser pulses for nonreciprocal writing in optically transparent materials," Opt. Express **18**, 24673–24678 (2010).
28. A. Braun, G. Korn, X. Liu, D. Du, J. Squier, and G. Mourou, "Self-channeling of high-peak-power femtosecond laser pulses in air," Opt. Lett. **20**, 73–75 (1995).
29. P. Bowlan, H. Valtna-Lukner, M. Lõhmus, P. Piksarv, P. Saari, and R. Trebino, "Measuring the spatiotemporal field of ultrashort Bessel-X pulses," Opt. Lett. **34**, 2276–2278 (2009).
30. Y. Vidne and M. Rosenbluh, "Spatial modes in a PCF fiber generated continuum," Opt. Express **13**, 9721–9728 (2005).
31. M. Bass, E. W. Van Stryland, D. R. Williams, and W. L. Wolfe, *Handbook of Optics* (McGraw-Hill, 2001).
32. U. Fuchs, U. Zeitner, and A. Tünnermann, "Ultra-short pulse propagation in complex optical systems," Opt. Express **13**, 3852–3861 (2005).
33. J. Ratner, G. Steinmeyer, T. C. Wong, R. Bartels, and R. Trebino, "Coherent artifact in modern pulse measurements," Opt. Lett. **37**, 2874–2876 (2012).
34. M. Rhodes, G. Steinmeyer, J. Ratner, and R. Trebino, "Pulse-shape instabilities and their measurement," Laser Photon. Rev. **7**, 557–565 (2013).

35. M. Rhodes, G. Steinmeyer, and R. Trebino, "Standards for ultrashort-laser-pulse-measurement techniques and their consideration for self-referenced spectral interferometry [Invited]," Appl. Opt. **53**, D1–D11 (2014).
36. P. Bowlan, P. Gabolde, A. Shreenath, K. McGresham, R. Trebino, and S. Akturk, "Crossed-beam spectral interferometry: a simple, high-spectral-resolution method for completely characterizing complex ultrashort pulses in real time," Opt. Express **14**, 11892–11900 (2006).
37. M. Miranda, M. Kotur, P. Rudawski, C. Guo, A. Harth, A. L'Huillier, and C. L. Arnold, "Spatiotemporal characterization of ultrashort laser pulses using spatially resolved Fourier transform spectrometry," Opt. Lett. **39**, 5142–5145 (2014).
38. F. Eilenberger, A. Brown, S. Minardi, and T. Pertsch, "Imaging cross-correlation FROG: measuring ultrashort, complex, spatiotemporal fields," Opt. Express **21**, 25968–25976 (2013).
39. P. Gabolde and R. Trebino, "Single-shot measurement of the full spatiotemporal field of ultrashort pulses with multispectral digital holography," Opt. Express **14**, 11460–11467 (2006).
40. Z. Guang, M. Rhodes, M. Davis, and R. Trebino, "Complete characterization of a spatiotemporally complex pulse by an improved single-frame pulse-measurement technique," J. Opt. Soc. Am. B **31**, 2736–2743 (2014).
41. K. W. DeLong, R. Trebino, and D. J. Kane, "Comparison of ultrashort-pulse frequency-resolved-optical-gating traces for three common beam geometries," J. Opt. Soc. Am. B **11**, 1595–1608 (1994).
42. P. Gabolde and R. Trebino, "Self-referenced measurement of the complete electric field of ultrashort pulses," Opt. Express **12**, 4423–4429 (2004).
43. L. Yu and M. K. Kim, "Wavelength-scanning digital interference holography for tomographic three-dimensional imaging by use of the angular spectrum method," Opt. Lett. **30**, 2092–2094 (2005).
44. M. Takeda, H. Ina, and S. Kobayashi, "Fourier-transform method of fringe-pattern analysis for computer-based topography and interferometry," J. Opt. Soc. Am. **72**, 156–160 (1982).
45. S. Akturk, M. Kimmel, P. O'Shea, and R. Trebino, "Extremely simple device for measuring 20-fs pulses," Opt. Lett. **29**, 1025–1027 (2004).
46. P. Gabolde and R. Trebino, "Single-frame measurement of the complete spatio-temporal intensity and phase of ultrashort laser pulse(s) using wavelength-multiplexed digital holography," J. Opt. Soc. Am. B **25**, A25–A33 (2008).
47. Z. Guang and R. Trebino, "Complete spatiotemporal measurement of ultrashort pulses emerging from multi-mode optical fiber," in *CLEO: Science and Innovations*, OSA Technical Digest (online) (Optical Society of America, 2015), paper SM2L.7.
48. G. P. Agrawal, *Nonlinear Fiber Optics* (Academic, 2007).
49. R. W. Boyd, *Nonlinear Optics* (Academic, 2003).
50. S. Akturk, X. Gu, P. Gabolde, and R. Trebino, "The general theory of first-order spatio-temporal distortions of Gaussian pulses and beams," Opt. Express **13**, 8642–8661 (2005).
51. S. Akturk, X. Gu, E. Zeek, and R. Trebino, "Pulse-front tilt caused by spatial and temporal chirp," Opt. Express **12**, 4399–4410 (2004).
52. A. M. Weiner, "Femtosecond pulse shaping using spatial light modulators," Rev. Sci. Instrum. **71**, 1929–1960 (2000).
53. P. Bowlan, U. Fuchs, R. Trebino, and U. D. Zeitner, "Measuring the spatiotemporal electric field of tightly focused ultrashort pulses with sub-micron spatial resolution," Opt. Express **16**, 13663–13675 (2008).